

# Optical Enhancement by Gold Nanoring-Nanodisk Plasmonic Structures for Light Sensing Applications

Ahmad Aziz Darweesh\*, Dhaidan Khalaf Kafi, Hamid Ahmed Fayyadh

Department of Medical Physics, College of Applied Science, University of Fallujah, Anbar, IRAQ.

\*Correspondent contact: [ahmad.darweesh@uofallujah.edu.iq](mailto:ahmad.darweesh@uofallujah.edu.iq)

## Article Info

Received  
25/05/2022

Accepted  
26/06/2022

Published  
30/12/2022

## ABSTRACT

We design and numerically model a 3D nanoring-nanodisk structure and evaluate the effect of the ring and the disk radii size within the presented structure on the optical enhancement. Nanoring-nanodisk is a powerful structure for enhancing the local electric field for photo-sensing applications. We present an enhanced local electric field from the UV to IR wavelength range using the proposed structure with fixed nanogap. It shows a strong dependence on the disk radius of the structure. In addition, two distinct peaks have different plasmonic vibrational modes appearing in the spectrum. These modes are revealed by 3D surface charge and local electric field distributions. Moreover, our calculations reveal that the smaller disk radius with a larger ring radius can generate more optical enhancement.

**KEYWORDS:** Nanoring-nanodisk, plasmonic, optical enhancement.

## الخلاصة

قمنا بتصميم ونمذجة هيكل نانوحلقة-نانوقرص ثلاثي الأبعاد رقمياً ودراسة تأثير نصف قطر الحلقة ونصف قطر القرص داخل الهيكل المقدم على التحسين الضوئي. يعتبر الهيكل نانوحلقة-نانوقرص واحد من أنواع كثيرة من الهياكل التي يستخدم لتحسين المجال الكهربائي المحلي والذي بدوره يستعمل في تطبيقات المتحسسات الضوئية. في هذه البحث نحسب المجال الكهربائي المحلي المحسن من نطاق الطول الموجي للأشعة فوق البنفسجية إلى الأشعة تحت الحمراء باستخدام الهيكل المقترح وباستخدام فتحة نانوية ثابتة الحجم فاصلة بين الحلقة والقرص. أظهرت النتائج ان المجال الكهربائي المحسن يعتمد اعتماداً قوياً على نصف قطر القرص للهيكل. بالإضافة إلى ذلك، بينت الحسابات أنه كلما قل نصف قطر القرص مع زيادة في نصف قطر الحلقة فإن المجال الكهربائي المحسن يزداد. علاوة على ذلك، ظهرت في الطيف قمتان متميزتان أساسيتان كل واحدة لها نمط اهتزازي مختلف. تم الكشف عن هذه الانماط الاهتزازية بواسطة توزيعات ثلاثية الأبعاد للشحنة السطحية وتوزيعات المجال الكهربائي المحلي.

## INTRODUCTION

When an electromagnetic wave (light) is incident on a piece of metal, the free electrons will vibrate harmonically with the light. This vibration can be presented as plasmonic modes, due to the interaction or coupling between the free electrons and the light, which depends on the frequency of the light. Basically, there are two main types of plasmons: surface and localized plasmons. The former type occurs when the size of plasmonic materials, such as gold, silver, copper, or aluminum, is hundreds of nanometers with flat surfaces. However, the latter type occurs when the size of the plasmonic materials is less than a hundred nanometers with curved surfaces. In addition, the generation of both types significantly depends on the shape of plasmonic materials and the surrounding media [1-3]. The plasmonic

phenomenon was utilized for years to enhance the incident light to many orders of magnitude and hence strengthen the reflected electromagnetic signals [4-6]. This technique is used in many applications, for example, surface-enhanced Raman scattering (SERS), biosensors, plasmonic photo-voltaic, plasmonic laser, photodetectors, single-molecule detection, and metasurfaces. Gold is used as a plasmonic material to design the nanostructure, This plasmonic metal is very common in the VIS and IR applications due to its optical properties that depend on the incident wavelength [7-10].

In these applications, different nanostructures were used to generate the highest possible optical enhancement, which in turn enhances the devices response. For instance, most prior work has studied the most common structures such as nanospheres,

nanodimers, nanomonomers, nanorods, nanodisks, and nanorings; others are nanomaterials, nanooctamers, nanocubes, and nanoflowers [11-22].

This paper aims to study the effect of the disk and ring radii of the gold nanoring-nanodisk plasmonic structure on optical enhancement. Usually, researchers used this type of structure to enhance the incident light by changing the disk radius and the gap space with a fixed ring radius. However, in this paper, we namely fix the gap space and change the radii of the disk and the ring at the same time. Our proposed structure is freely suspended in the air.

## MATERIALS AND METHODS

To investigate the plasmonic response of a 3D gold ring-disk nanostructure, the near field (local field) was considered. The local field is calculated in a volume of 2 nm above the metal surface [12]. The 3D ring-disk nanostructure comprises two parts: a gold nanoring centered by a gold nanodisk and separated by a fixed nanogap ( $g$ ) as shown in Figure 1. We use a model created by COMSOL to ease the analytical calculations. We employed the experimental results to describe the optical properties of the gold (frequency-dependent) [23]. In the model, we fix the radius of the entire structure ( $R_{tot}$ ) at 60 nm, which is equal to the summation of the ring radius ( $R_R$ ), disk radius ( $R_D$ ), and gap space ( $g$ ).

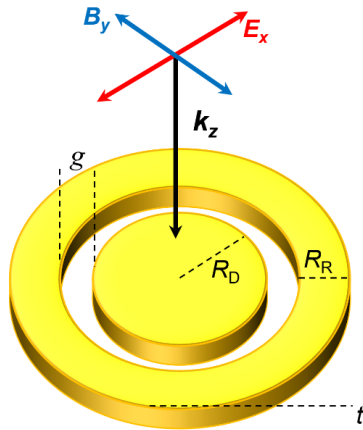


**Figure 1.** 3D schematic diagram of monomer ring-disk plasmonic nanostructure. The structure consists of the disk and ring with radii ( $R_D$ ) and ( $R_R$ ), respectively. ( $g$ ) and ( $t$ ) are the separated nanogap (between the disk and the ring) and the thickness of the structure, respectively. TM polarized light is incident from the top of the structure. The nanostructure is surrounded by a dielectric material (air).

The structure thickness is fixed at 15 nm. The disk radius is swept from 15 to 50 nm with a 5 nm step

size. TM polarized light is employed to hit the structure normally from the top. Eq. (1) is used to compute and visualize the charge distribution on the nanoring-nanodisk surfaces [12]. Surface charge distributions can illustrate the electric pole configurations.

$$\rho = \varepsilon_0(n \cdot E) \quad (1)$$

Where  $\rho$  is the surface charge,  $\varepsilon_0$  is the vacuum permittivity,  $n$  is the ring-disk surface normal vector, and  $E$  is the near electric field. The three-dimensional electrodynamic computations are carried out using COMSOL Multiphysics 5.4. The electromagnetic field distributions are calculated using the radio frequency (RF) module with a frequency domain interface study. To prevent scattered waves from returning to the model space, a 300 nm thick perfectly matched layer (PML) is employed to surround the entire nanostructure. We set the gap space  $g$  to 2 nm and use a 10 nm step size to sweep the incident wavelength from 400 to 1600 nm. We set the incident electric field as  $E_0 = 1\text{V/m}$  and optical enhancement as  $(E_{local}/E_0)^2$ , where  $E_{local}$  is the local electric field.

## RESULTS AND DISCUSSION

Figure 2 shows the logarithms of the near field enhancement log (EF) of a gold nanoring-nanodisk structure as a function of the incident wavelength ( $\lambda$ ). For all calculations, we fixed  $g$  at 2 nm and  $R_{tot}$  at 60 nm. We gradually increase  $R_D$  from 15 to 30 nm with a step size of 5 nm. We sweep the wavelength from 400 to 1600 nm with 10 nm step size.

Two distinct resonant peaks appear in each curve, showing dominant strong plasmon modes at  $\lambda_D=625$  nm in the visible regime and others belong to nanoring at  $\lambda_{R1}=1000$  nm,  $\lambda_{R2}=1150$  nm,  $\lambda_{R3}=1325$  nm, and  $\lambda_{R4}=1500$  nm, respectively, in the infrared regime. Increasing  $R_D$  can reduce the enhanced electric field around the structure and in the gap space gradually. For the disk, the plot shows that the resonant peaks at  $\lambda_D=625$  nm decrease with increasing  $R_D$ . For the ring, in addition, in the enhancement peaks, there is decreasing and redshift. That could be attributed to the different plasmonic resonant modes, as will be further explained in the next paragraphs.

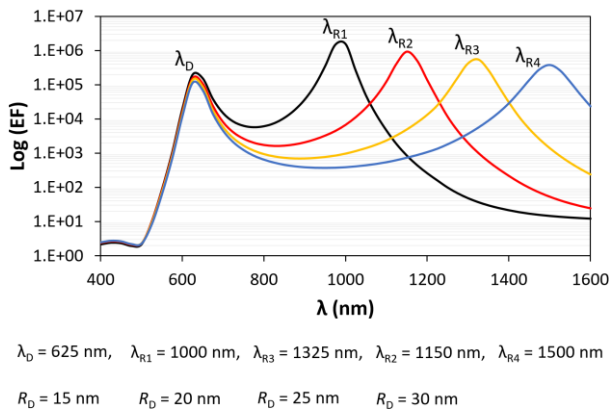


**Figure 2.** A plot of electric field enhancement (EF) as a function of the incident wavelength ( $\lambda$ ). Only four different nanodisk radii were shown ( $R_D = 15, 20, 25,$  and  $30$  nm). Two resonant peaks appear in each curve. One belongs to nanodisk at  $\lambda=625$  nm and others belong to nanoring at  $\lambda_{R1}=1000$  nm,  $\lambda_{R2}=1150$  nm,  $\lambda_{R3}=1325$  nm, and  $\lambda_{R4}=1500$  nm, respectively.

Figure 3a shows a linear relationship between the enhanced electric field and the disk radius ( $R_D$ ) at  $\lambda=625$  nm when we sweep  $R_D$  from 15 nm to 50 nm with a step size of 5 nm. In Figure 3b a linear relationship between the enhanced electric field and the resonant peaks at resonant wavelengths is presented as well; it shows that decreasing  $R_R$  can significantly reduce the enhanced electric field, due to the changing in the resonant plasmonic vibration modes.

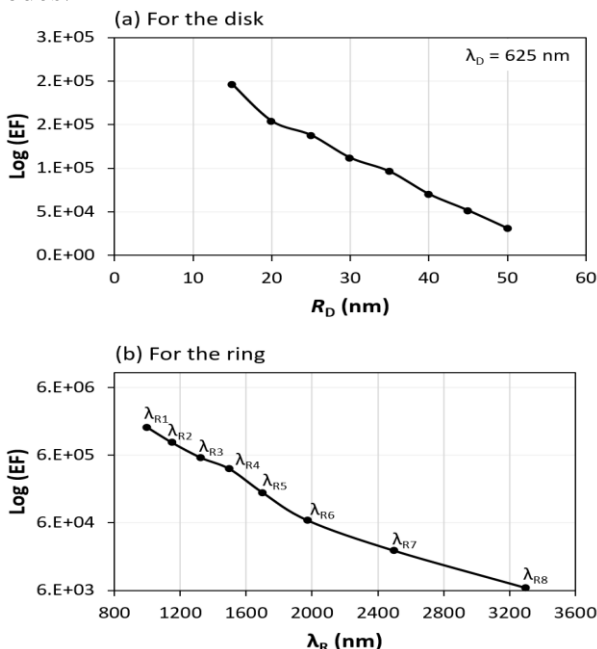


**Figure 3.** Plots of electric field enhancements (EF) as a function of (a) disk radius  $R_D$  and (b) resonant wavelengths ( $\lambda_R$ ). In (a), the near electric field at resonant peaks with  $R_D = 15-50$  nm with 5 nm step size at fixed incident wavelength  $\lambda_D=625$  nm is presented. In (b), the near electric field is shown

as a function of resonant wavelengths for the ring with  $R_D=15-50$  nm with 5 nm step size.

Figure 4 illustrates the surface charge distributions for the ring-disk nanostructures as shown in Figure 3a. Figure 4a shows that the disk vibrates with plasmonic dipole modes (fundamental mode) that gives the highest enhancement, whereas, Figure 4b-4e shows that the disk vibrates with quadrupole plasmonic modes. This type of mode could decrease the enhancement significantly. In addition, increasing  $R_D$  leads to decreases  $R_R$ , which in turn reduces the enhancement peaks of the ring.

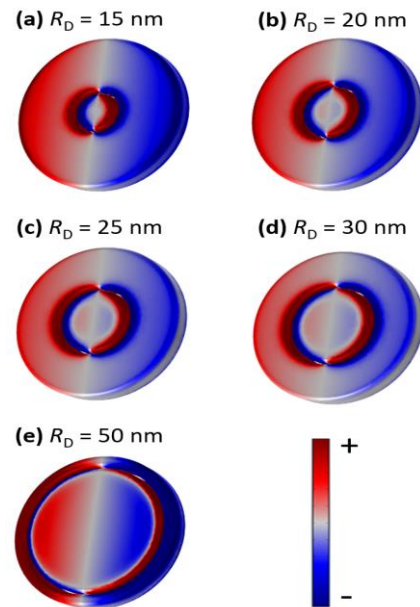


**Figure 4.** 3D surface charge distributions for the ring-disk nanostructures at resonant peaks of the disk at fixed incident wavelength  $\lambda_D = 625$  nm. The charge distributions are presented for different  $R_D$ .

Figure 5 illustrates the electric field distribution for each case in Figure 4. It is clear that smaller  $R_D=15$  nm (Figure 5a) can generate a stronger electric field, especially in the gap region. This could be attributed to the dipole mode that is created on the nanodisk surface. Figure 5 a-e generates almost the same local electric field around the nanostructure. Figure 6 is the 3D surface charge distributions that appear in Figure 3 b. The resonant plasmonic vibration modes at these wavelengths ( $\lambda_{R1} = 1000$  nm,  $\lambda_{R2} = 1150$  nm,  $\lambda_{R3} = 1325$  nm, and  $\lambda_{R4} = 1500$  nm, respectively) are completely different. In Figure 6 a, the plasmonic modes for the ring and the disk are dipole modes. For this reason, we notice that the highest resonant peaks occur at  $R_D = 15$  nm and  $\lambda_{R1} = 1000$  nm. However, the resonant peaks (at the other resonant wavelengths  $\lambda_{R2}, \lambda_{R3},$

$\lambda_{R4}$ , and  $\lambda_{R8}$ ) become lesser when  $R_D$  increases. This is due to the quadrupole vibration mode of the nanoring.

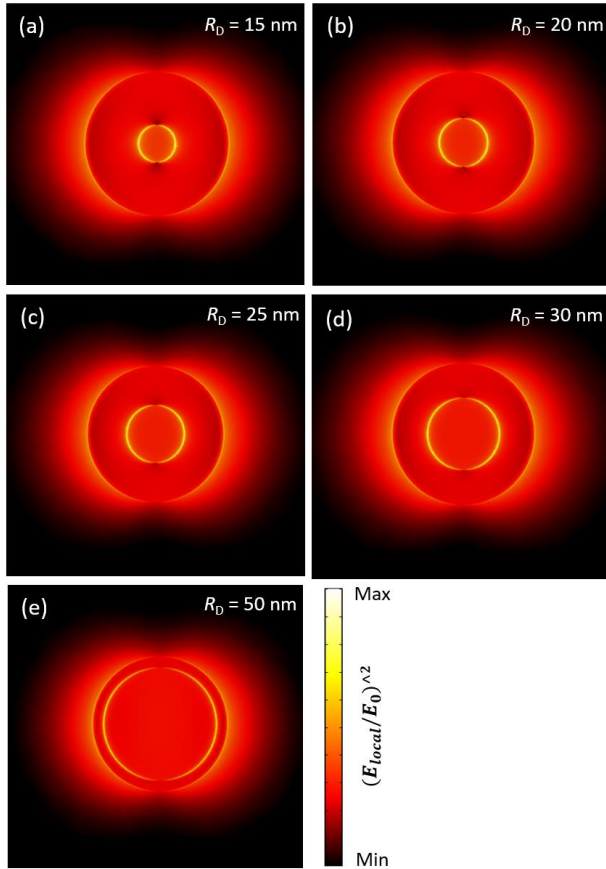


**Figure 5.** Local electric field distributions for the ring-disk nanostructures at the same structures are in Figure 4.

In addition, the main difference between Figure 6 and Figure 4 is the vibrational modes of the disk. In Figure 6, the disk vibrates with dipole mode no matter how large is the radius of the disk, however, in Figure 4 only at  $R_D = 15$  nm, the disk vibrates with dipole mode. This is the reason that makes the resonant peaks of the ring ( $\lambda_{R1}$ ,  $\lambda_{R2}$ ,  $\lambda_{R3}$ , and  $\lambda_{R4}$ ) are higher than the resonant peaks at  $\lambda_D$ , see Figure 2.

Figure 7 illustrates the electric field distributions for each case in Figure 6. The stronger local electric field in the gap space and around the structure appears in Figure 7a. And the electric field becomes weaker when the  $R_D$  becomes larger, see Figure 7b-7e.

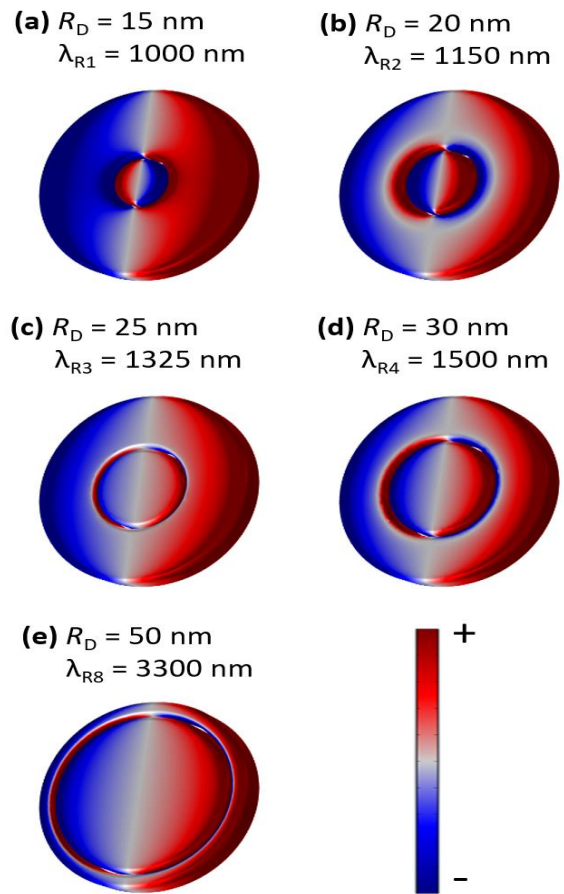


**Figure 6.** 3D surface charge distributions for the ring-disk nanostructures at first resonant peak of the ring at different resonant incident wavelength  $\lambda_R$ .

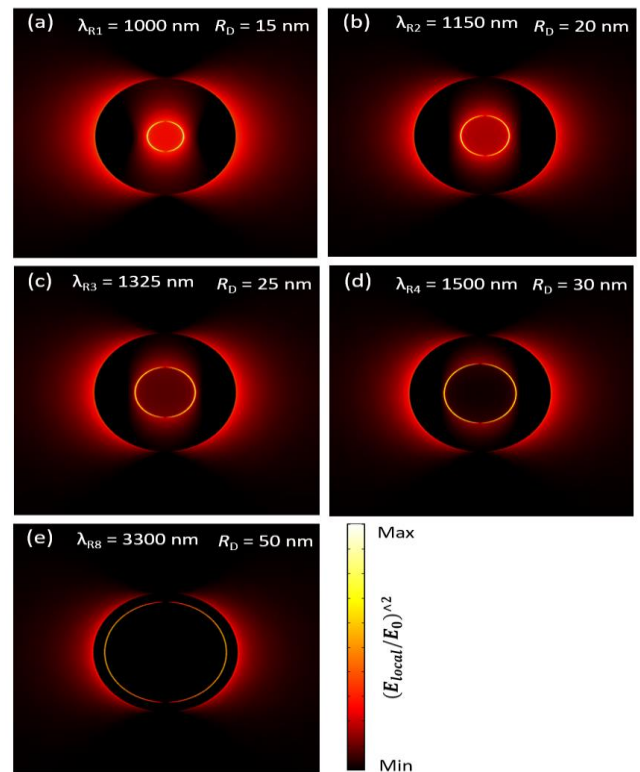


**Figure 7.** Local electric field distributions for the ring-disk nanostructures at the same structures are in Figure 6.

## CONCLUSIONS

The surface plasmon resonances of a nanoring-nanodisk structure were studied for the structure's ability to enhance the local electric field. A Strong electric field enhancement was observed when the radius of the disk reduces with fixed gap space. All resonant plasmonic peaks for the disk appeared in the VIS regime ( $\lambda_D = 625$  nm) whereas all resonant plasmonic peaks for the ring appeared in the IR regime ( $\lambda_{R1} = 1000$  nm,  $\lambda_{R2} = 1150$  nm,  $\lambda_{R3} = 1325$  nm, and  $\lambda_{R4} = 1500$  nm) with redshift. The strongest enhanced electric field for the disk was created in the gap space and on the disk surfaces at resonant peaks but only in the gap space at resonant peaks for the ring. A significant difference observed in the strength of the enhanced electric field is purely due to the type of plasmonic modes which illustrate the coupling nature of ring-disk nanostructures.

**Disclosure and conflict of interest:** The authors declare that they have no conflicts of interest.

## REFERENCES

- [1] P. L. Stiles, J. A. Dieringer, N. C. Shah, and R. P. Van Duyne, "Surface-enhanced Raman spectroscopy," *Annu Rev Anal Chem (Palo Alto Calif)* 1, 601-626 (2008). <https://doi.org/10.1146/annurev.anchem.1.031207.112814>
- [2] B. N. Khlebtsov and N. G. Khlebtsov, "Multipole Plasmons in Metal Nanorods: Scaling Properties and Dependence on Particle Size, Shape, Orientation, and Dielectric Environment," *J. Phys. Chem. C* 111, 11516-11527 (2007). <https://doi.org/10.1021/jp072707e>
- [3] C. Noguez, "Surface Plasmons on Metal Nanoparticles: The Influence of Shape and Physical Environment," *J. Phys. Chem. C* 111, 3806-3819 (2007). <https://doi.org/10.1021/jp066539m>
- [4] S. J. Bauman, A. A. Darweesh, and J. B. Herzog, "Surface-enhanced Raman spectroscopy substrate fabricated via nanomasking technique for biological sensor applications," in *Advanced Fabrication Technologies for Micro/Nano Optics and Photonics IX* (SPIE, 2016), Vol. 9759, pp. 170-177. <https://doi.org/10.1117/12.2213086>
- [5] A. M. Funston, C. Novo, T. J. Davis, and P. Mulvaney, "Plasmon Coupling of Gold Nanorods at Short Distances and in Different Geometries," *Nano Lett.* 9, 1651-1658 (2009). <https://doi.org/10.1021/nl900034v>
- [6] E. K. Payne, K. L. Shuford, S. Park, G. C. Schatz, and C. A. Mirkin, "Multipole Plasmon Resonances in Gold Nanorods," *J. Phys. Chem. B* 110, 2150-2154 (2006). <https://doi.org/10.1021/jp056606x>
- [7] X. Wang, Y. Wu, X. Wen, J. Zhu, X. Bai, Y. Qi, and H. Yang, "Surface plasmons and SERS application of Au nanodisk array and Au thin film composite structure," *Opt Quant Electron* 52, 238 (2020). <https://doi.org/10.1007/s11082-020-02360-2>
- [8] M. S. Islam, J. Sultana, M. Biabanifard, Z. Vafapour, M. J. Nine, A. Dinovitsner, C. M. B. Cordeiro, B. W.-H. Ng, and D. Abbott, "Tunable localized surface plasmon graphene metasurface for multiband superabsorption and terahertz sensing," *Carbon* 158, 559-567 (2020). <https://doi.org/10.1016/j.carbon.2019.11.026>
- [9] Y. Liu and F. Luo, "Spatial Raman mapping investigation of SERS performance related to localized surface plasmons," *Nano Res.* 13, 138-144 (2020). <https://doi.org/10.1007/s12274-019-2586-2>
- [10] F. A. A. Nugroho, D. Albinsson, T. J. Antosiewicz, and C. Langhammer, "Plasmonic Metasurface for Spatially Resolved Optical Sensing in Three Dimensions," *ACS Nano* 14, 2345-2353 (2020). <https://doi.org/10.1021/acsnano.9b09508>
- [11] D. T. Debu, D. T. Debu, D. T. Debu, Q. Yan, Q. Yan, Q. Yan, A. A. Darweesh, M. Benamara, and G. Salamo, "Broad range electric field enhancement of a plasmonic nanosphere heterodimer," *Opt. Mater. Express, OME* 10, 1704-1713 (2020). <https://doi.org/10.1364/OME.10.001704>
- [12] A. A. Darweesh, D. T. Debu, S. J. Bauman, and J. B. Herzog, "Near- and Far-Field Plasmonic Enhancement by Asymmetric Nanosphere Heterodimers," *Plasmonics* (2022). <https://doi.org/10.1007/s11468-022-01650-7>
- [13] P. Zhao, Y. Chen, Y. Chen, S. Hu, H. Chen, W. Xiao, G. Liu, Y. Tang, J. Shi, Z. He, Y. Luo, and Z. Chen, "A MoS<sub>2</sub> nanoflower and gold nanoparticle-modified surface plasmon resonance biosensor for a sensitivity-improved immunoassay," *J. Mater. Chem. C* 8, 6861-6868 (2020). <https://doi.org/10.1039/D0TC00556H>
- [14] B. Sun, Z. Wang, Z. Liu, X. Tan, X. Liu, T. Shi, J. Zhou, and G. Liao, "Tailoring of Silver Nanocubes with Optimized Localized Surface Plasmon in a Gap Mode for a Flexible MoS<sub>2</sub> Photodetector," *Advanced Functional Materials* 29, 1900541 (2019). <https://doi.org/10.1002/adfm.201900541>
- [15] X. Wang, X. Bai, Z. Pang, H. Yang, and Y. Qi, "Investigation of surface plasmons in Kretschmann structure loaded with a silver nano-cube," *Results in Physics* 12, 1866-1870 (2019). <https://doi.org/10.1016/j.rinp.2019.02.002>
- [16] I. Zorić, M. Zäch, B. Kasemo, and C. Langhammer, "Gold, Platinum, and Aluminum Nanodisk Plasmons: Material Independence, Subradiance, and Damping Mechanisms," *ACS Nano* 5, 2535-2546 (2011). <https://doi.org/10.1021/nn102166t>
- [17] P. Nordlander, C. Oubre, E. Prodan, K. Li, and M. I. Stockman, "Plasmon Hybridization in Nanoparticle Dimers," *Nano Lett.* 4, 899-903 (2004). <https://doi.org/10.1021/nl049681c>

- [18] H.-P. Liang, L.-J. Wan, C.-L. Bai, and L. Jiang, "Gold Hollow Nanospheres: Tunable Surface Plasmon Resonance Controlled by Interior-Cavity Sizes," *J. Phys. Chem. B* 109, 7795-7800 (2005). <https://doi.org/10.1021/jp045006f>
- [19] D. W. Brandl, N. A. Mirin, and P. Nordlander, "Plasmon Modes of Nanosphere Trimers and Quadrumers," *J. Phys. Chem. B* 110, 12302-12310 (2006). <https://doi.org/10.1021/jp0613485>
- [20] L. Lin, M. Zapata, M. Xiong, Z. Liu, S. Wang, H. Xu, A. G. Borisov, H. Gu, P. Nordlander, J. Aizpurua, and J. Ye, "Nanooptics of Plasmonic Nanomatryoshkas: Shrinking the Size of a Core-Shell Junction to Subnanometer," *Nano Lett.* 15, 6419-6428 (2015). <https://doi.org/10.1021/acs.nanolett.5b02931>
- [21] E. K. Payne, K. L. Shuford, S. Park, G. C. Schatz, and C. A. Mirkin, "Multipole Plasmon Resonances in Gold Nanorods," *J. Phys. Chem. B* 110, 2150-2154 (2006). <https://doi.org/10.1021/jp056606x>
- [22] A. M. Funston, C. Novo, T. J. Davis, and P. Mulvaney, "Plasmon Coupling of Gold Nanorods at Short Distances and in Different Geometries," *Nano Lett.* 9, 1651-1658 (2009). <https://doi.org/10.1021/nl900034v>
- [23] P. B. Johnson and R. W. Christy, "Optical Constants of the Noble Metals," *Phys. Rev. B* 6, 4370-4379 (1972). <https://doi.org/10.1103/PhysRevB.6.4370>

## How to Cite

A. A. Darweesh, D. K. . Kafi, and H. A. Fayyadh, "Optical Enhancement by Gold Nanoring-Nanodisk Plasmonic Structures for Light Sensing Applications", *Al-Mustansiriyah Journal of Science*, vol. 33, no. 4, pp. 112–117, Dec. 2022.